Rapid Prediction of High-Alpha Unsteady Aerodynamics of Slender-Wing Aircraft

L. E. Ericsson* and H. H. C. King†
Lockheed Missiles & Space Company, Inc., Sunnyvale, California 94088

Most aerospace vehicles, although designed for hypersonic cruise at low angles of attack, often have to perform rapid maneuvers at high angles of attack from low supersonic down to low subsonic speeds. There is, therefore, a need for rapid prediction of the nonlinear high-alpha vehicle dynamics of slender-wing aircraft in that speed range. The present paper describes such a prediction method, which can account for the nonlinear dynamic effects of leading-edge vortices at angles of attack, yaw, and roll. A comparison with existing experimental results shows that the accuracy of the prediction is satisfactory for preliminary design as long as breakdown of the leading-edge vortices does not occur.

Nomenclature

A	=	aspect ratio, b^2/S
$A(x)$	=	apparent cross-sectional area
b	=	wing span
$\bar{c}$	=	reference length, $2c_o/3$ for a delta wing
c_o	=	slender-wing root chord
k	=	reduced roll frequency, $\omega b/2U_\infty$
L	=	lift; coefficient $C_L = L/(\rho_\infty U_\infty^2/2)S$
l	=	rolling moment; coefficient $C_l = l/(\rho_\infty U_\infty^2/2)Sb$
M	=	Mach number
M_p	=	pitching moment; coefficient $C_m = M_p/(\rho_\infty U_\infty^2/2)S\bar{c}$
N	=	normal force; coefficient $C_N = N/(\rho_\infty U_\infty^2/2)S$
P	=	static pressure; coefficient $C_p = (P - P_\infty)/(\rho_\infty U_\infty/2)$
p	=	roll rate
q	=	pitch rate
S	=	reference area (= projected wing area)
s	=	local semispan
t	=	time
U	=	horizontal velocity
$\bar{U}$	=	mean convection velocity
X	=	horizontal inertial space coordinate
x	=	axial body-fixed coordinate
y	=	spanwise body-fixed coordinate
Z	=	vertical inertial space coordinate
z	=	vertical body-fixed coordinate
α	=	angle of attack
α_o	=	trim angle of attack
β	=	sideslip angle
Δt	=	timelag
ζ	=	dimensionless z coordinate, z/c_o
η	=	dimensionless y coordinate, y/s
θ	=	pitch perturbation
θ_{le}	=	apex half angle
θ_{te}	=	trailing-edge sweep angle
Λ	=	leading-edge sweep angle, $\pi/2 - \theta_{le}$
ξ	=	dimensionless x coordinate, $(x_A - x)/c_o$
ρ	=	air density
ϕ	=	roll angle
ω, $\bar{\omega}$	=	angular frequency, $\bar{\omega} = \omega c_o/U_\infty$

Subscripts

A	=	apex
a	=	attached flow
cg	=	center of gravity
le	=	leading edge
s	=	separated flow
te	=	trailing edge
v	=	vortex
∞	=	freestream conditions

Superscript

$\bar{}$	=	integrated mean values, e.g., centroid of aerodynamic loads

Differential Symbols

$\dot{\theta}$	=	$\partial\theta/\partial t$; $\ddot{\phi} = \partial^2\phi/\partial t^2$; $C_{m\theta} = \partial C_m/\partial\theta$
$C_{m\dot{\theta}}$	=	$C_{mq} + C_{m\dot{\alpha}} = \partial C_m/\partial(\bar{c}\dot{\theta}/U_\infty)$: $C_{mq} = \partial C_m/\partial(\bar{c}q/U_\infty)$
C_{lp}	=	$\partial C_l/\partial(bp/2U_\infty)$: $C_{l\dot{\beta}} = \partial C_l/\partial(b\dot{\beta}/2U_\infty)$

Introduction

THE complexity of the flowfield on aircraft and aircraft-like configurations at high angles of attack prohibits the use of numerical computational methods for preliminary design. Because of the continual changes in the early design, a purely experimental method cannot be used either. One needs rapid computational methods to guide the early stages of preliminary design until a firmer design has evolved on which experimental and numerical methods can be applied.

A fast prediction method, developed earlier for the nonlinear unsteady longitudinal aerodynamics of sharp-edged delta wings,[1] has been extended to include the roll degree of freedom. The predicted high-alpha aerodynamics are compared with existing experimental results for slender wings and wing-body configurations.

Analysis

The simple flow concept by Polhamus,[2] i.e., the leading-edge suction analogy, has been remarkably successful in predicting the nonlinear lift generated by the leading-edge vortex on slender wings at high angles of attack. This is true not only for simple delta wings, but also for so-called double deltas, and the method also predicts experimentally observed Mach number effects. Because the vortex lift is, in reality, depend-

Presented as Paper 90-3037 at the 8th Applied Aerodynamics Conference, Seattle, WA, June 18–20, 1990; received Sept. 10, 1990, revision received Dec. 21, 1990; accepted for publication Dec. 27, 1990. Copyright © 1991 by L. E. Ericsson. Published by the American Institute of Aeronautics and Astronautics, Inc., with permission.

*Retired. Presently Engineering Consultant. Fellow AIAA.
†Presently with ETAK, Inc., Menlo Park, California. Member AIAA.

ent on upstream flow conditions, and the leading-edge suction depends only on local conditions, the flow concept cannot be applied to the unsteady aerodynamics. However, it is a very useful tool for determination of the static loads and was used as a starting point in the earlier analysis of slender-wing pitch damping.[1] The present analysis extends this earlier analysis to include the roll degree of freedom. Because of space limitations, the reader is referred to Ref. 3 for the full details of the present analysis. Only the part of the analysis addressing the extension to include the roll degree of freedom will be given in full here.

Roll Damping Analysis

The momentum theory applied to the pitch oscillations in Ref. 1 will now be applied to the roll degree of freedom ϕ. Again, the delta wing is considered to be at $\alpha = 0$ in the freestream velocity $U_\infty \cos\alpha_0$. Thus, there are no loads induced by the roll deflection ϕ, only by the roll rate $\dot\phi = p$.

In the present case, Fig. 1 is applied to a strip of $\eta =$ constant with $A(X)$ substituted by $\Delta A(X)$, as is indicated by the sketch in Fig. 2. $\Delta A(X)$ is expressed as the portion of the full cross section, i.e., the contribution from the opposite wing half is included

$$\Delta A(X) = 2s^2\sqrt{1-\eta^2}\,d\eta \tag{1}$$

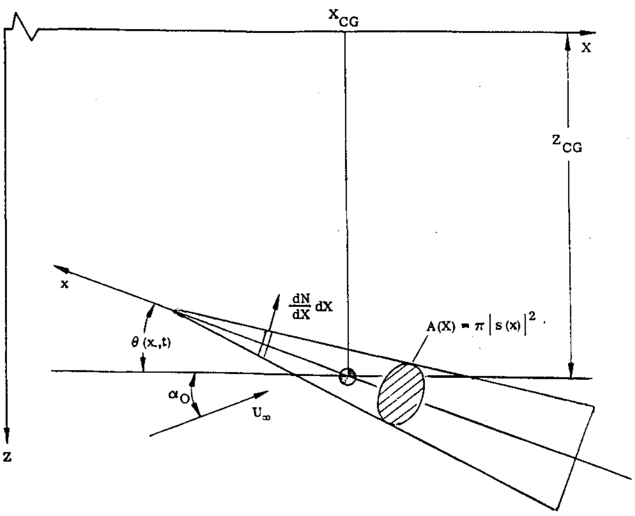

Fig. 1 Vehicle coordinate system.

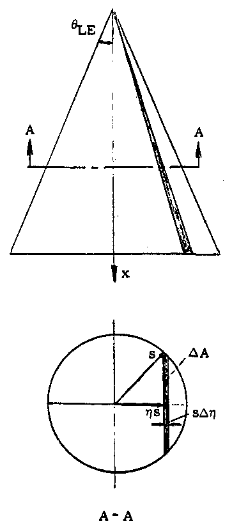

Fig. 2 Apparent mass of rolling delta wing.

Applying the pitch-plane analysis in Ref. 1 (Fig. 1) gives the strip load in Fig. 2. Noticing that $z = z_{cg} + \eta s\phi$ gives the following:

$$\frac{1}{\cos^2\alpha_0}\frac{d\Delta C_N}{dx} = \left(-\frac{\partial}{\partial x} + \frac{1}{U_\infty\cos\alpha_0}\frac{\partial}{\partial t}\right) \times \left[\frac{2\Delta A(x)}{S}\frac{\eta s\dot\phi}{U_\infty\cos\alpha_0}\right] = -\frac{\partial}{\partial x}\left[\frac{2\Delta A(x)}{S}\frac{\eta s\dot\phi}{U_\infty\cos\alpha_0}\right] + \frac{2\Delta A(x)}{S}\frac{\eta s\ddot\phi}{U_\infty^2\cos^2\alpha_0} \tag{2}$$

The corresponding rolling moment is

$$\frac{\Delta C_l}{\cos^2\alpha_0} = -\int_{x_{te}}^{x_A}\frac{d\Delta C_N}{dx}\frac{\eta s}{b}\,dx \tag{3}$$

Combining Eqs. (2) and (3) gives

$$\frac{\Delta C_l}{\cos^2\alpha_0} = \int_{x_{te}}^{x_A}\frac{2\Delta A(x)}{Sb}\frac{\eta^2 s^2\dot\phi}{U_\infty\cos\alpha_0} - \int_{x_{te}}^{x_A}\frac{2\Delta A(x)}{Sb}\frac{\eta^2 s^2\ddot\phi}{U_\infty^2\cos^2\alpha_0}\,dx \tag{4}$$

Noticing that $\dot\phi = p$, $s(x_A) = 0$, $s(x_{te}) = b/2$, and $S = (b/2)^2\cot\theta_{le}$, Eqs. (1) and (4) combine to give

$$\Delta C_{l_p} = \frac{\partial\Delta C_l}{\partial(pb/2U_\infty)} = -(2\cos\alpha_0\tan\theta_{le})\eta^2\sqrt{1-\eta^2}\,d\eta \tag{5}$$

That is,

$$C_{l_p} = -2\cos\alpha_0\tan\theta_{le}\int_0^1\eta^2\sqrt{1-\eta^2}\,d\eta = -\frac{\pi}{8}\cos\alpha_0\tan\theta_{le} \tag{6}$$

Equation (6) is valid only for $M_\infty = 1$, where the slender-wing value $C_{N\alpha 0}$ is valid. For other Mach numbers, the modified derivative[4] $C_{N\theta a} = K_{Ma}C_{N\alpha 0}$ has to be used, and Eq. (6) takes the following form:

$$C_{l_p} = -\frac{\pi A}{32}K_{Ma}\cos\alpha_0 \tag{7a}$$

$$K_{Ma} = \frac{2}{1 + A\bar\beta/4 + \sqrt{1+(A\bar\beta/4)^2}} \tag{7b}$$

$$\bar\beta = \sqrt{|1-M_\infty^2|} \tag{7c}$$

Separated Flow Contribution

During roll oscillations, the leading edge experiences a local upwash sp, orthogonal to the wing plane. For small reduced frequencies, $(pb/2U_\infty)^2 << 1$, the corresponding angle of attack is

$$\Delta\alpha = \frac{\xi pb}{2U_\infty}\cos\alpha_0 \tag{8}$$

The corresponding vortex-induced normal force is

$$C_{N_v} = \pi K_{M_v}\sin^2(\alpha_0 + \Delta\alpha) \tag{9a}$$

$$K_{Mv} = \sqrt{1-(A\beta/4)^2}\begin{cases}1 & : \ 0 \le M_\infty < 1 \\ K_{Ma}^2 & : \ 1 \le M_\infty \le \sqrt{1+(A/4)^{-2}}\end{cases} \tag{9b}$$

When considering the corresponding rolling moment, the spanwise location of the vortex-induced load components becomes important. As the roll rate induces an α/θ_{le} distribution along the leading edge that is very similar to that for the pitching rate,[5] similarly large effects on the vortex location are expected (Fig. 3). Although the longitudinal camber does not seem to have a significant effect on the magnitude of the vortex-induced suction peak, it does affect its spanwise location. The pitch-rate-induced effect on the longitudinal α/θ_{le} distribution is similar to that produced by making the leading-edge planform more convex, which produces a marked outboard movement of the leading-edge vortex[6] (Fig. 4).

The rolling moment corresponding to the normal force defined by Eq. (9) can be written as follows (noting that $\bar{y}/b = \bar{\xi}\bar{\eta}/2$):

$$C_{lv} = -0.5\ C_{Nv}[\varepsilon\bar{\xi}_v\bar{\eta}_\alpha + (1-\varepsilon)\bar{\xi}_v\bar{\eta}_v] \tag{10}$$

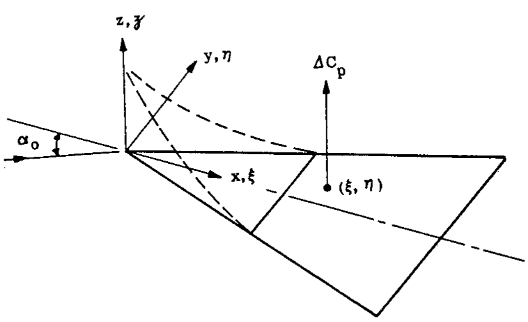

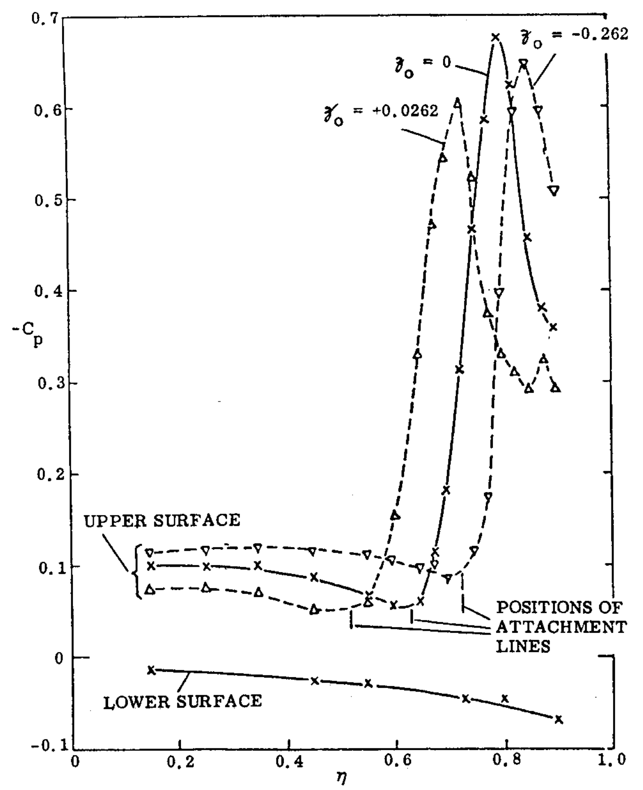

Fig. 3 Spanwise pressure distribution at ξ = 0.583 for deformed delta wing at α_o = 5 deg.[5]

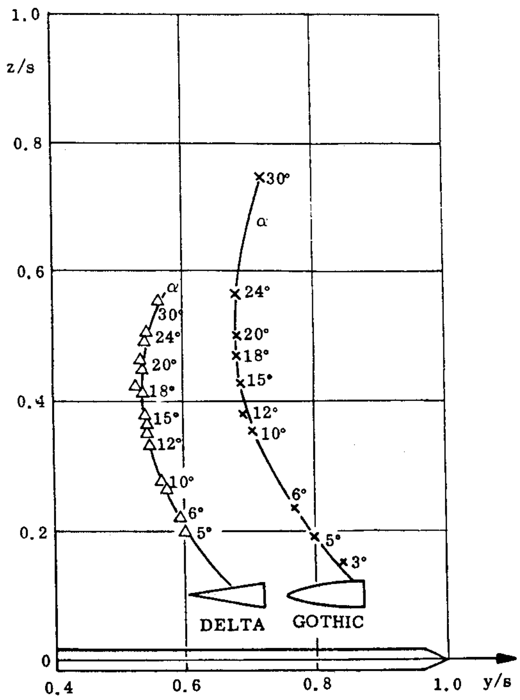

Fig. 4 Spanwise vortex position at the trailing edge of slender sharp-edged wings.[6]

Combining Eqs. (8–10) gives

$$C_{lpv} = \frac{\partial C_{lv}}{\partial(pb/2U_\infty)} = -\frac{1}{2}\left\{\frac{\partial C_{Nv}}{\partial(pb/2U_\infty)}\right.$$

$$\left.[\varepsilon\bar{\xi}_v\bar{\eta}_a + (1-\varepsilon)\bar{\xi}_v\bar{\eta}_v] - C_{Nv}(1-\varepsilon)\bar{\xi}_v\frac{\partial\bar{\eta}_v}{\partial(pb/2U_\infty)}\right\} \tag{11a}$$

$$\frac{\partial C_{Nv}}{\partial(pb/2U_\infty)} = 2\pi K_{Mv}\bar{\xi}_v \sin\alpha_0\cos^2\alpha_0 \tag{11b}$$

$$C_{Nv} = \pi K_{Mv}\sin^2\alpha_0 \tag{11c}$$

It remains to determine $\partial\bar{\eta}_v/\partial(pb/2U_\infty)$. The results in Fig. 3 give a longitudinal camber $\Delta\alpha = 0.052 = 3.0$ deg. That is, for $\alpha_o = 5$ deg, $\Delta\alpha/\tan\alpha \approx \Delta\alpha/\alpha = 0.6$, which together with $\Delta\eta_v = 0.07$ from Fig. 3 gives

$$\frac{\partial\bar{\eta}_v}{\partial(\Delta\alpha/\tan\alpha)} \approx 0.12 \tag{12}$$

For a pitching delta wing

$$\Delta\alpha(q) = \frac{c_0 q}{U_\infty} \tag{13}$$

For a rolling delta wing one obtains

$$\Delta\alpha(p) = \frac{pb}{2U_\infty}\cos\alpha_0 \tag{14}$$

Thus,

$$\frac{\partial\bar{\eta}_v}{\partial(pb/2U_\infty)} = \frac{\partial\bar{\eta}_v}{\partial(\Delta\alpha/\tan\alpha)}\frac{\cos\alpha_0}{\tan\alpha_0} = 0.12\cos\alpha_0\cot\alpha_0 \tag{15}$$

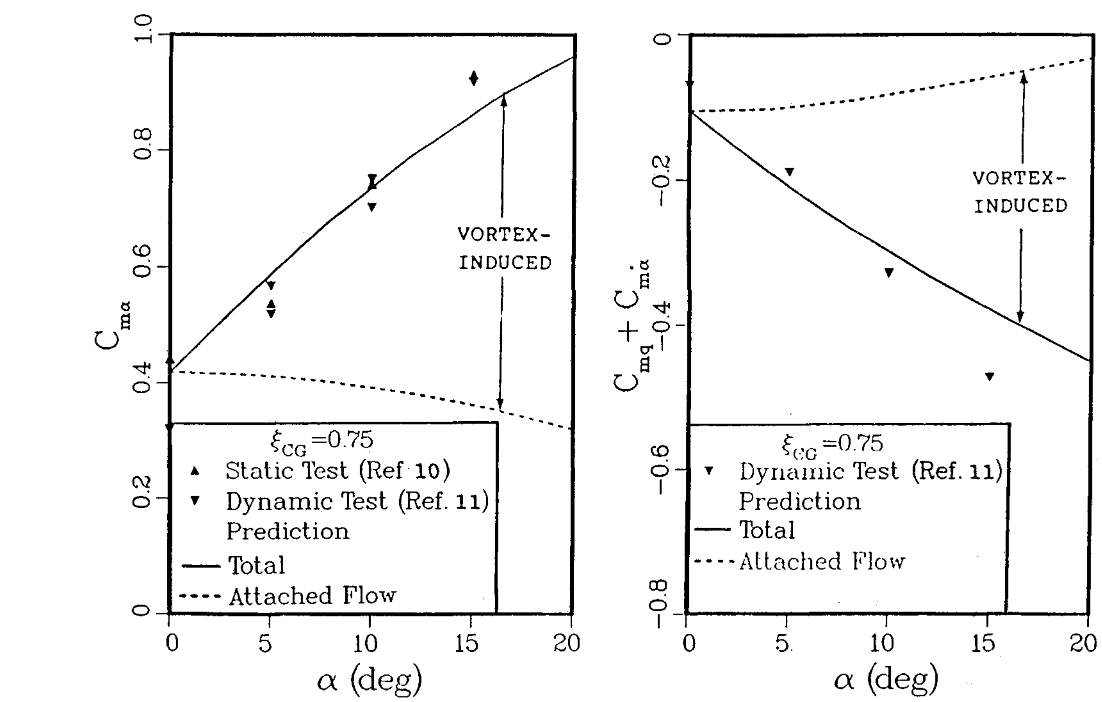

Fig. 5 Stability derivatives of a 69.6-deg delta wing.

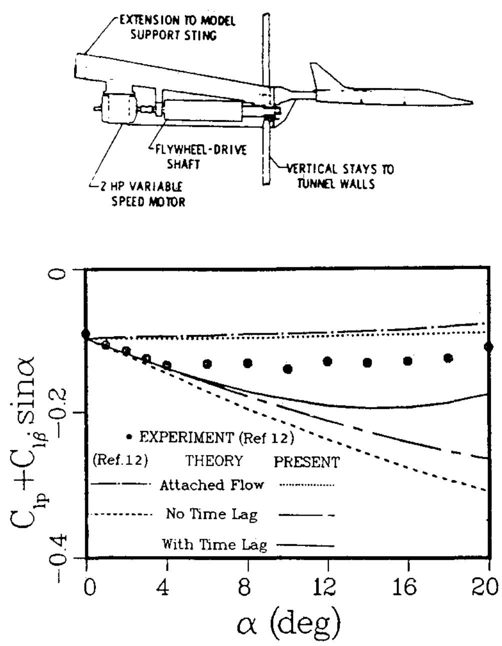

Fig. 6 Roll damping of a 74-deg delta wing.

Combining Eqs. (11) and (15), with $\varepsilon = 0.3$, gives

$$C_{lp\nu} = -\pi K_{M\nu}\bar{\xi}_\nu[\bar{\xi}_\nu(0.3\bar{\eta}_a + 0.7\bar{\eta}_\nu) + 0.042] \sin \alpha_0 \cos^2 \alpha_0 \tag{16}$$

The effects considered so far, Eqs. (7) and (16), are those generated by the roll-rate-induced change of the local, instantaneous flow conditions. There is, in addition, the time-dependent effect of a change of the apex flow conditions, similar to that for the damping in pitch.[1] The roll angle ϕ produces the following modifications of the effective angles of attack and sideslip:

$$\bar{\alpha} = \arctan(\tan \alpha_0 \cos \phi) \tag{17a}$$

$$\bar{\beta} = \pm\arcsin(\sin \alpha_0 \sin \phi) \tag{17b}$$

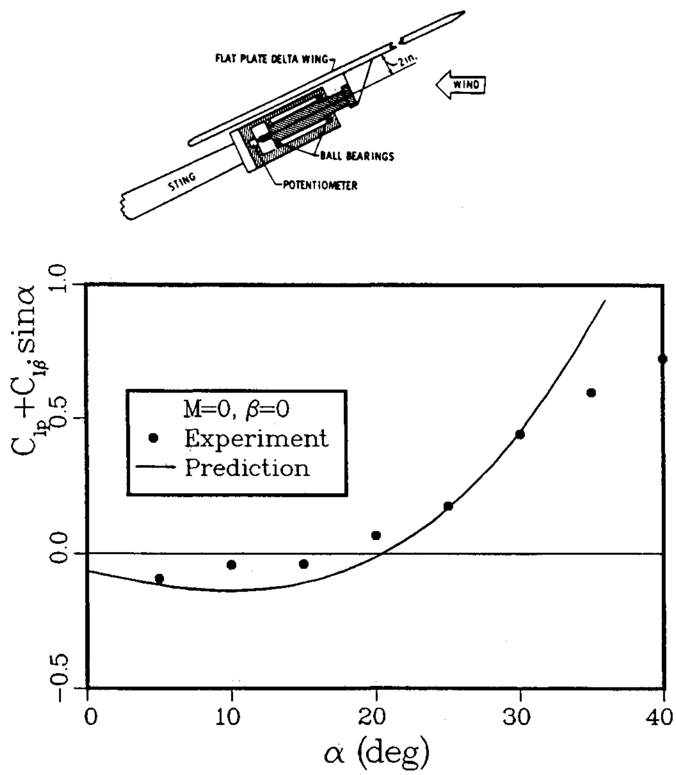

Fig. 7 Roll damping of an 80-deg delta wing.

For small roll deflections, $|\phi| < 10$ deg, Eqs. (17) simplify to

$$\bar{\alpha} \approx \alpha_0 \tag{18a}$$

$$\bar{\beta} \approx \pm\phi \sin \alpha_0 \tag{18b}$$

Thus, the roll-induced sideslip at apex induces the following rolling moment

$$\Delta^i C_{l\nu}(t) = C_{l\beta\nu} \sin \alpha_0\, \phi(t - \Delta t) \tag{19a}$$

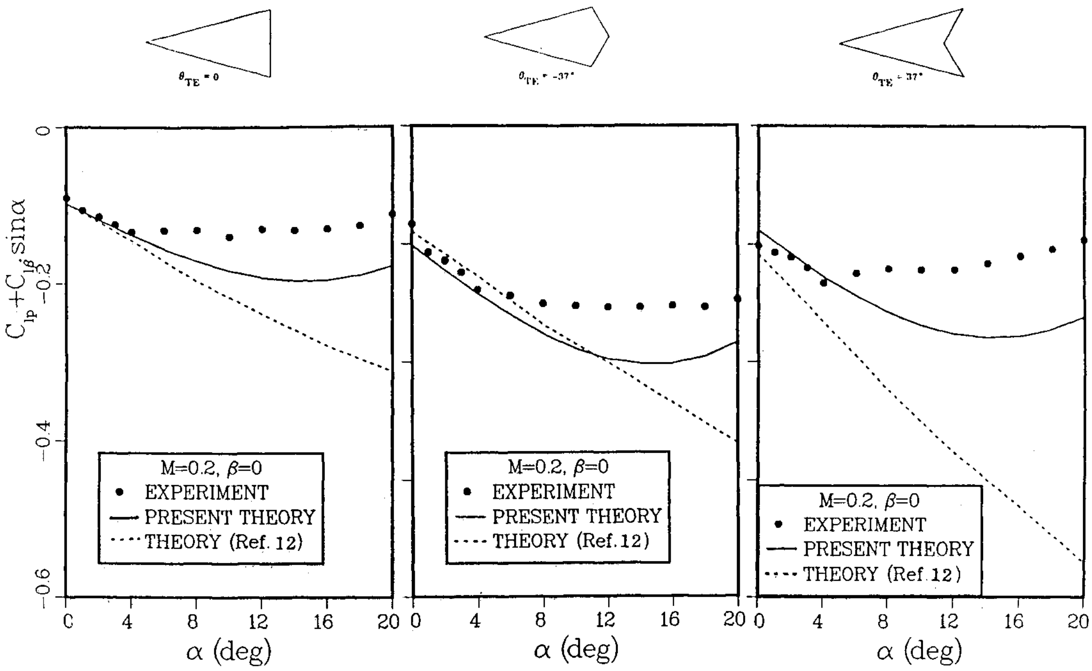

Fig. 8 Effect of trailing-edge sweep on roll damping of wings with 74-deg leading-edge sweep.

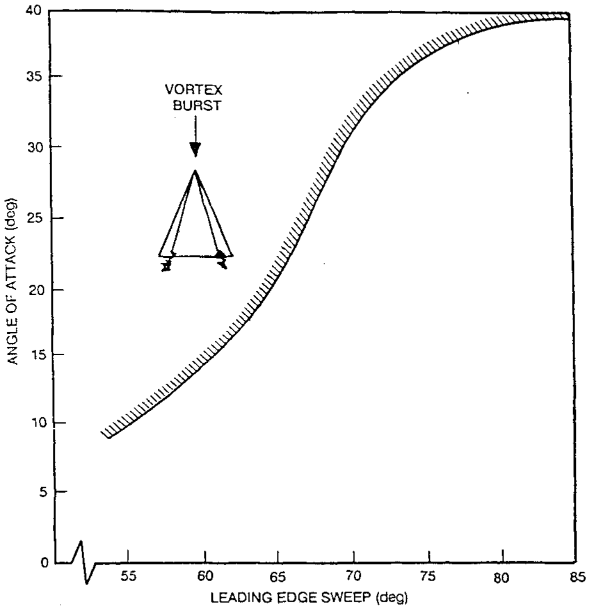

Fig. 9 Angle-of-attack/leading-edge-sweep boundary for delta wing vortex breakdown.[2]

where

$$\Delta t = \bar{\xi}_v c_0 / \bar{U}_v \tag{19b}$$

Thus, Eqs. (19) can be written as

$$\Delta^i C_{l\nu}(t) = C_{l\beta\nu} \sin \alpha_0 [\phi - \bar{\xi}_v c_0 \dot{\phi} / \bar{U}_v]$$

$$= C_{l\beta\nu} \sin \alpha_0 \left[\phi - \bar{\xi}_v \frac{b\dot{\phi}}{2U_\infty} \cot \theta_{le} \right] \tag{20}$$

where $\bar{U}_v$ is the average convection velocity of the vortex reaction to the change of flow conditions at apex. For the lateral aerodynamics, $\bar{U}_v \approx U_\infty$ according to experiments,[7] whereas $\bar{U}_v \approx U_\infty/0.75$ for the longitudinal aerodynamics.[1] For moderate roll rates, $(b\dot{\phi}/2U_\infty)^2 << 1$, $\phi(t - \Delta t)$ can be expressed by a Taylor expansion, and Eq. (20) can be written as

$$\Delta^i C_{l\dot{\phi}\nu} = \frac{\partial \Delta^i C_{l\nu}}{\partial(b\dot{\phi}/2U_\infty)} = -C_{l\beta\nu} \bar{\xi}_v \sin \alpha_0 \cot \theta_{le} \tag{21}$$

With $C_{l\beta\nu}$ as defined in Ref. 8, Eq. (21) gives the following expression for $\Delta^i C_{l\dot{\phi}\nu}$

$$\Delta^i C_{l\dot{\phi}\nu} = \frac{2\pi K_{M\nu}}{A} \tan \alpha_0 \sin^2 \alpha_0$$

$$\times \left[0.7 \bar{\eta}_v \bar{\xi}_v \left(\frac{2\bar{\eta}_v - 1}{\bar{\eta}_v} \frac{4}{A} - \frac{A}{4} \right) + 0.3 \bar{\eta}_a \bar{\xi}_a \left(\frac{4}{A} - \frac{A}{4} \right) \right] \tag{22}$$

Effect of Trailing-Edge Sweep

The effective delta-wing treatment applied in Ref. 8 will work also in the case of the roll damping, with one exception. The C_{l_p} derivative in Eqs. (6) and (7) is valid only for a true delta wing. As the slender-wing (or body) theory only produces lift for increasing cross-sectional area, i.e., increasing semispan $s(x)$ in the present case, the only correction needed to Eqs. (6) and (7) is to substitute the use of $S = (b/2)^2 \cot \theta_{le}$ with $(b/2)^2 (\cot \theta_{le} - \tan \theta_{te})$. Thus, Eq. (7a) becomes

$$C_{l_p} = -\frac{\pi A}{32} K_{Ma} \frac{\cos \alpha_0}{1 - \tan \theta_{te} \tan \theta_{le}} \tag{23}$$

with K_{Ma} defined in Eqs. (7b) and (7c)

Discussion of Results

The longitudinal stability characteristics for a 69.6-deg delta wing ($A = 1.484$) shown in Fig. 5 demonstrate the opposite vortex-induced effects on static and dynamic stability caused by convective time lag effects.[1] Considering the problem of support interference,[9] the agreement between prediction and experiment[10,11] is completely satisfactory.

As expected, the vortex-induced loads also have a pronounced influence on the stability characteristics in roll, as is illustrated in Fig. 6 for the roll damping of a 74-deg delta wing.[12] The effect of the local, roll-induced velocity at the leading edge more than doubles the attached flow damping at $\alpha > 10$ deg. However, when adding the effect of the time lag, which occurs before the vortex has reacted to the roll-induced change of the flow conditions at the apex, an effect neglected in the theory of Ref. 12, the total roll damping is reduced substantially. The remaining deviation between the present prediction and experiment[12] is the likely result of interference from the bulky support system (see insert in Fig. 6). This may also be the reason for the deviation between prediction and experiment[13] for the roll damping of an 80-deg delta wing at low angles of attack (Fig. 7). However, the deviation at $\alpha > 35$ deg is caused by vortex burst, the effect of which is not (yet) included in the present prediction. Figure 8 shows that the prediction of the effect of trailing-edge sweep by the present theory agrees much better with experiment[12] than that by the theory of Ref. 12. It is noteworthy that the deviation between present prediction and experiment is rather insensitive to the trailing-edge sweep, in sharp contrast to the large sensitivity exhibited by the prediction of Ref. 12. Such insensitivity would be expected if the deviation is caused by support interference on the leading-edge vortices.

Support interference becomes a serious problem at high angles of attack, when a bulky support can cause premature breakdown of leading-edge vortices.[9] Figure 9 shows how vortex burst is delayed to higher and higher angles of attack as the leading-edge sweep is increased.[2] The boundary in Fig. 9 is used to determine at what angle of attack the present prediction ceases to be valid, indicated by a vertical bar. The support needed for high-alpha testing is rather bulky and can cause premature vortex burst with results[14] such as those illustrated in Fig. 10. When the leading-edge sweep is more modest than the 74 and 80 deg of the models in Figs. 6–8, a sideslip angle of a certain magnitude may be needed, as is illustrated in Fig. 11. In this case, the roll-induced effective sideslip on the windward, dipping wing half, Eqs. (17) and (18), will promote support interference. Thus, when comparing the present prediction with experiment, the effective leading-edge sweep is taken as $\Lambda_{\mathrm{eff}} = \Lambda - \beta$.

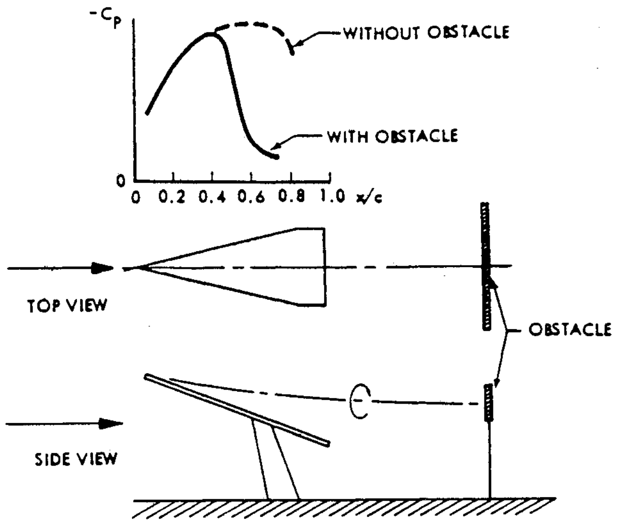

Fig. 10 Vortex breakdown on a 75-deg delta wing caused by downstream obstacle.[14]

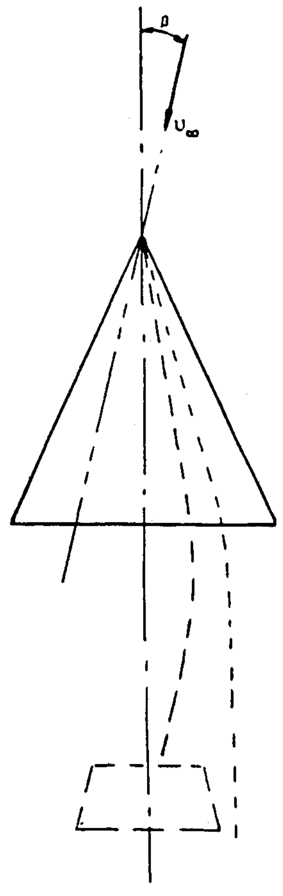

Fig. 11 Effect of sideslip on support interference.

Aerospace Vehicle Results

So far, only results for pure delta wings have been discussed. However, the current interest is the low-speed aerodynamics of hypersonic aerospace vehicles. Figure 12 shows that the prediction of the low-speed lateral stability characteristics of a hypersonic boost-glide configuration is in satisfactory agreement with experiment.[15] For the 78-deg delta wing, vortex breakdown does not occur until $\alpha = 38$ deg, according to the experimental results[2] in Fig. 9. Assuming that $\Delta\phi = 10$ deg (no information is available in Ref. 15) gives $\Lambda_{\mathrm{eff}} \approx 73$ deg, with associated vortex breakdown occurring at $\alpha \approx 35$ deg, the value used in the prediction in Fig. 12. The earlier deviation between prediction and experiment,[15] at $\alpha < 35$ deg, is probably caused by support interference.[16]

Figure 13 shows that the lateral stability characteristics measured in low-speed tests of a re-entry configuration with

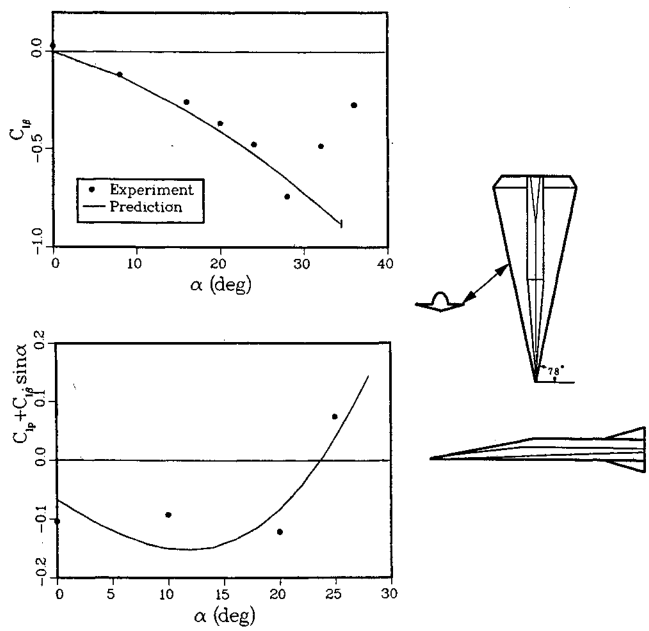

Fig. 12 Low-speed roll-stability characteristics of a hypersonic boost-glide configuration.

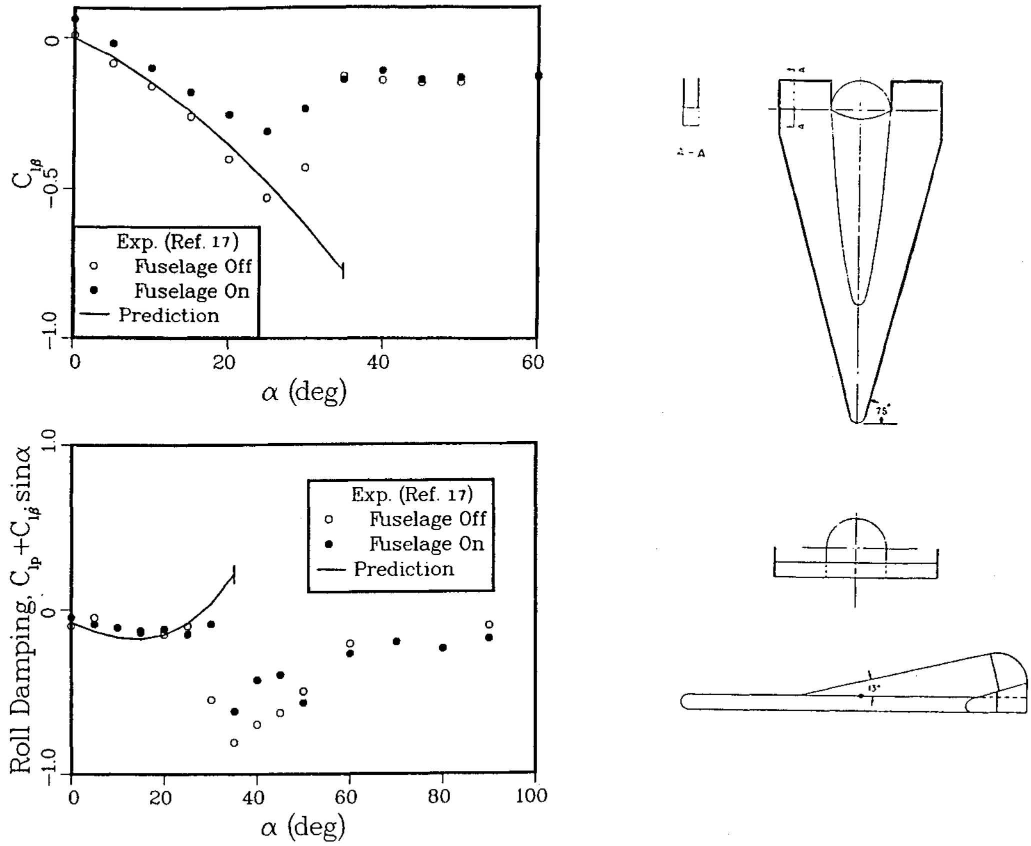

Fig. 13 Low-speed roll stability of a re-entry vehicle configuration with a thick 75-deg delta wing.

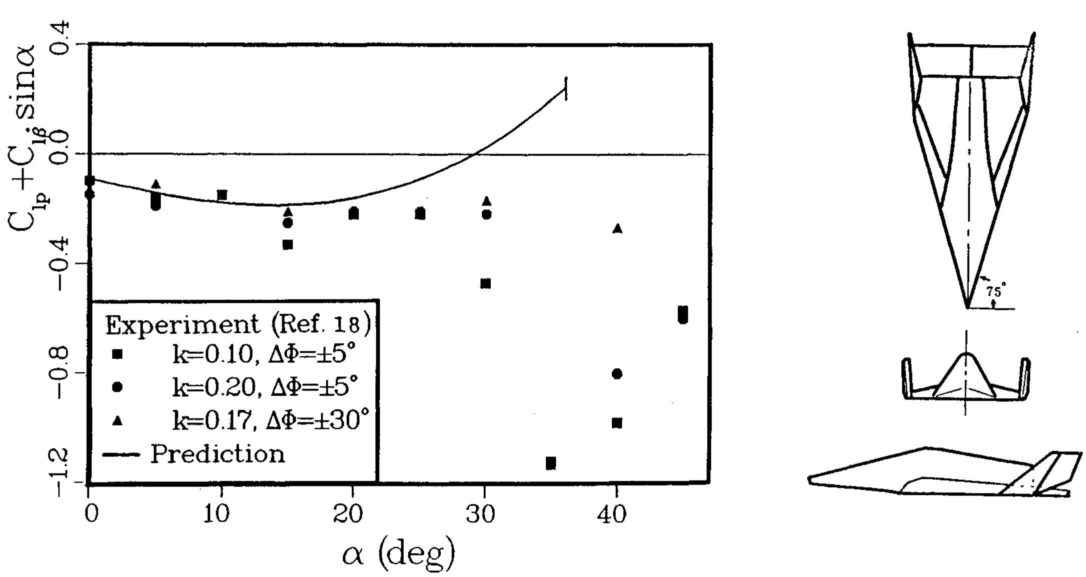

Fig. 14 Roll damping of a lifting re-entry vehicle with a 75-deg delta wing.

a thick, flat 75-deg delta wing[17] are also well predicted until vortex burst occurs. The fuselage is seen to influence the effect of burst but to have little effect on the stability characteristics at lower angles of attack. The figure illustrates how the effect of vortex burst is opposite on static and dynamic stability characteristics, $C_{l\beta}$ vs. $C_{lp} + C_{l\dot{\beta}} \sin \alpha$. It is the result of the time lag effect discussed earlier in connection with Fig. 5. Finally, Fig. 14 shows that the predicted roll damping of a lifting re-entry vehicle with a 75-deg delta wing is in good agreement with experiment[18] until vortex burst occurs, probably promoted by support interference. It is also possible that interaction between the leading-edge vortices and the tip fins can have promoted an early vortex breakdown. The small tip fins in Fig. 13 are less likely to have contributed to the early vortex burst. That is, support interference alone is the likely cause in that case.

Conclusions

The roll damping results presented here, combined with the static characteristics discussed in Ref. 19, show that the developed rapid prediction method produces results that are of sufficient accuracy for preliminary design of slender delta wing and wing-body configurations, as long as vortex breakdown does not occur.

Acknowledgment

This work was supported by the Lockheed Missiles & Space Company Independent Development Program.

References

[1]Ericsson, L. E., and Reding, J. P., "Unsteady Aerodynamic Analysis of Space Shuttle Vehicles, Part II; Steady and Unsteady Aerodynamics of Sharp-Edged Delta Wings," NASA CR-120123, Aug. 1973.

[2]Polhamus, E. C., "Predictions of Vortex-Lift Characteristics by Leading-Edge-Suction Analogy," *Journal of Aircraft*, Vol. 8, No. 4, 1971, pp. 193–199.

[3]Ericsson, L. E., and King, H. H. C., "Rapid Prediction of Slender-Wing Aircraft Dynamics," AIAA Paper 90-3037, Aug. 1990.

[4]Ericsson, L. E., and Reding, J. P., "Effect of Angle of Attack and Mach Number on Slender-Wing Unsteady Aerodynamics," *Journal of Aircraft*, Vol. 15, No. 6, 1978, pp. 358–365.

[5]Lambourne, N. C., Bryer, D. W., and Maybrey, J. F. M., "Pressure Measurements on a Model Delta Wing Undergoing Oscillatory Deformation," Aeronautical Research Council, Great Britain, NPL Aero Rept. 1314, March 1970.

[6]Werlé, H., "Vortices from Very Sender Wings," *La Recherche Aérospatiale*, No. 109, 1965, pp. 1–12.

[7]Lambourne, N. C., Bryer, D. W., and Maybrey, J. F. M., "The Behavior of the Leading-Edge Vortices over a Delta Wing Following a Sudden Change of Incidence," Aeronautical Research Council, Great Britain, R&M No. 3645, 1969.

[8]Ericsson, L. E., and Reding, J. P., "Approximate Nonlinear Wing Aerodynamics," *Journal of Aircraft*, Vol. 14, No. 12, 1977, pp. 1197–1204.

[9]Ericsson, L. E., and Reding, J. P., "Dynamic Support Interference in High Alpha Testing," *Journal of Aircraft*, Vol. 23, No. 12, 1986, pp. 889–896.

[10]Woodgate, L., and Halliday, A. S., "Measurement of Lift, Drag, and Pitching Moment on a Series of Three Delta Wings," Pt. 4, Aeronautical Research Council, Great Britain, R&M No. 3628, 1968.

[11]Woodgate, L., and Pugh, P. G., "Measurements of the Oscillatory Pitching Moment Derivatives on a Slender Sharp-Edged Delta Wing in Incompressible Flow," Pt. 2, Aeronautical Research Council, Great Britain, R&M No. 3628, 1968.

[12]Boyden, R. P., "Effect of Leading Edge Vortex Flow on the Roll Damping of Slender Wings," *Journal of Aircraft*, Vol. 8, No. 7, 1971, pp. 543–547.

[13]Nguyen, L. T., Yip, L., and Chambers, J. R., "Self-Induced Wing Rock of Slender Delta Wings," AIAA Paper 81-1883, Aug. 1981.

[14]Hummel, D., "Untersuchungen über das Aufplatzen der Wirbel an schlanken Delta Flügeln," *Z. f. Flugwissenschaften*, Vol. 3, Heft. 5, 1965, pp. 158–168.

[15]Paulson, J. W., and Shanks, R. E., "Investigation of Low-Subsonic Flight Characteristics of a Model of a Hypersonic Boost-Glide Configuration Having a 78° Delta Wing," NASA TND-894, May 1961.

[16]Ericsson, L. E., "Another Look at High-Alpha Support Interference," AIAA Paper 90-0188, Jan. 1990.

[17]Boisseau, P. C., "Investigations of the Low-Subsonic Flight Characteristics of a Model of a Reentry Vehicle with a Thick Flat 75° Swept Delta Wing and a Half-Cone Fuselage," NASA TN D-1007, Feb. 1962.

[18]Wall, G. M., and Shanks, R. E., "Investigation of the Low-Subsonic Flight Characteristics of a Model of a Reentry Configuration Having a 75° Delta Wing," NASA TM X-684, May 1962.

[19]Ericsson, L. E., and King, H. H. C., "Rapid Prediction of Slender-Wing-Aircraft Stability Characteristics," AIAA Paper 90-0301, Jan. 1990.

Recommended Reading from the AIAA
Progress in Astronautics and Aeronautics Series . . . AIAA

Thermal Design of Aeroassisted Orbital Transfer Vehicles

H. F. Nelson, editor

Underscoring the importance of sound thermophysical knowledge in spacecraft design, this volume emphasizes effective use of numerical analysis and presents recent advances and current thinking about the design of aeroassisted orbital transfer vehicles (AOTVs). Its 22 chapters cover flow field analysis, trajectories (including impact of atmospheric uncertainties and viscous interaction effects), thermal protection, and surface effects such as temperature-dependent reaction rate expressions for oxygen recombination; surface-ship equations for low-Reynolds-number multicomponent air flow, rate chemistry in flight regimes, and noncatalytic surfaces for metallic heat shields.

***TO ORDER:* Write, Phone or FAX:**
American Institute of Aeronautics and Astronautics,
c/o TASCO, 9 Jay Gould Ct., P.O. Box 753, Waldorf, MD 20604
Phone (301) 645-5643, Dept. 415 ▪ FAX (301) 843-0159

Sales Tax: CA residents, 7%; DC, 6%. For shipping and handling add $4.75 for 1–4 books (call for rates for higher quantities). Orders under $50.00 must be prepaid. Foreign orders must be prepaid. Please allow 4 weeks for delivery. Prices are subject to change without notice. Returns will be accepted within 15 days.

1985 566 pp., illus. Hardback
ISBN 0-915928-94-9
AIAA Members $54.95
Nonmembers $81.95
Order Number V-96